Predictions of Buoyancy-induced Flow in Asymmetrical Heated Rotating Cavity System

ABDUL FATAH ABBASI*, JAWAID DAUDPOTO*, AND MUHAMMAD SALEH JUMANI**

RECEIVED ON 17.05.2013 ACCEPTED ON 11.09.2013

ABSTRACT

This paper presents the finite difference solutions for buoyancy-induced flow in the asymmetrical heated rotating cavity system for the range of rotational Reynolds numbers Re_θ=6.13x10^5≤Re_θ=4.4x10^6 and the mass flow rates C_w≤28000≤C_w≤ 3000. All the simulations have been carried out through the CFD (Computational Fluid Dynamics) commercial code, ANSYS Fluent 12.0, by adopting axisymmetric, Steady-state and elliptic technique. Two well know models namely k-ε and the Reynolds stress models have been employed. The simulated results illustrate the important aspects of the heated rotating cavity flow system. The noteworthy influence of buoyancy-induced flow have been observed on the predicted stream lines, static temperature contours and the local Nusselt numbers for the rotating cavity space. A comparison of the predicted local Nusselt numbers for the hot and cold discs showed a good level of agreement with the measurements.

Key Words: **Rotating Cavity System, Low Reynolds Number Second Moment Closure, Buoyancy-Induced Flow.**

1. INTRODUCTION

The rotating cavity system with a super imposed cooling air flow has a relevance to the internal air cooling of gas turbine engine. The main purpose of this system is to keep the temperature of different engine components under safe operating limits. The internal cooling air is extracted from the main stream flow of the engine, which decreases the temperature of engine components and increases the turbine cycle efficiency. Childs, et. al. [1] revealed that about 20% of the engine main stream flow is utilized for the engine cooling purpose at the cost of 5% of fuel consumption. The minimum use of main stream air for cooling purpose has increased the turbine cycle efficiency of the engine. The correct calculations of buoyancy induced flow will help the researchers to devise an effective air cooling system for the future generation engines. In the heated rotating cavity system, the flow structure is distorted due to the buoyancy-induced effects. Result of that heat is transferred from the hot disc to cold disc through the transport of fluid. Previous research work provided the experimental and computational research papers for the rotating disc flow system. The flow visualization experiments of Owen and Onur [2] showed the parametric effects on the nature of flow, which was oscillating and chaotic in the nature. Memon [3] also illustrated the same behaviour of the rotationally-induced buoyancy parameter on heat transfer calculations by considering the rotational Grashof number. Mirzaee, et. al. [4]

* Assistant Professor, Department of Mechanical Engineering, Mehran University of Engineering & Technology, Jamshoro.
** Assistant Professor, Department of Industrial Engineering & Management, Mehran University of Engineering & Technology, Jamshoro.

presented numerical and experimental studies regarding the rotating cavity flows for the rotational Reynolds number $Re_\theta = 1.5x10^6$ and $C_w = 3000$. Their work illustrated the uniform tangential velocity profiles in the centre of cavity and corroborated the significant effects of vortices (free and forced) in this region. Kilic [5] investigated the significant effects of various parameters (G, Re_θ and C_w) on the predicted flow structures and heat transfer calculations in the rotating cavity system with peripheral air flow conditions. Karabay, et. al. [6] reported theoretical and computational studies of the flow and heat transfer in pre-swirl rotating disc system by considering the turbulent flow parameters such as, pre-swirl ratio, mass flow rate (C_w) and rotational Reynolds number (Re_θ). These parameters also are considered in the work of Lock, et. al. [7] for the heat transfer measurements. Later on Owen, et. al. [8,9] investigated experimentally the effects of buoyancy-induced parameter on the heat transfer calculations in the rotating cavity system. They pointed out the three multi-cell structures of cyclonic and anti-cyclonic vortices. Recently, Vinod Kumar, et. al. [10] presented numerical study of rotating cavities with radial inflow by using two popular eddy viscosity models (the Spalart-Allmaras and the k-ε) and a Reynolds stress model. They have mentioned the some shortcomings of former model and improved results of later model. Similarly, in the present study main focus has been given to both models, the k-ε and the Reynolds stress model. Both the models are employed to investigate the buoyancy-induced flow parameter and its effects on the heat transfer calculations. Therefore, the range of rotational Reynolds numbers, $Re_\theta = 6.13x10^5 \leq Re_\theta = 4.4x10^6$ and the mass flow rates, $C_w \leq 28000 \leq C_w \leq 3000$ are considered for the predictions of heat and fluid flow in the heated rotating cavity system. All the predictions have been carried out by implementing the CFD commercial code, ANSYS Fluent by activating two low Reynolds number turbulence models, the k-ε model and the Reynolds stress model, so-called the low Reynolds number second moment closure. The simulations have been compared with the measurement of Mark-II rig TFMRC (Thermo Fluid Mexchanics Research Centre), University of Sussex (Memon, [3]).

2. PROBLEM SPECIFICATION AND NUMERICAL METHOD

The geometry of the simulation domain is identical to the experimental rig of Mark-II Memon [3], as presented in Fig. 1. The dimensions of the geometry and applied boundary conditions are given as under:

b=427.5mm, r_i =44.5mm, s=56.0mm and G= 0.138

U=V=W=0 at z=0, r_i<r<b, V=W=0, U=U_i at z=0, 0<r< r_i

U=V=0, W=Ωr at z=s, 0<r<b, U=W=0, V=V_o at r=b, 0<z<S_c

where b, r_i, s and G are the cavity outer radius, inlet radius, axial spacing and gap ratio respectively.

The boundary conditions at the inlet and outlet show that the cooling air enters the rotating cavity axially passing through a central hole in the upstream disc and impinges directly on the downstream disc (hot disc) and developed a wall jet along the disc in radial direction. The temperature distribution on the hot disc is assumed to be non-uniform and increasing radially and reaches the maximum value of

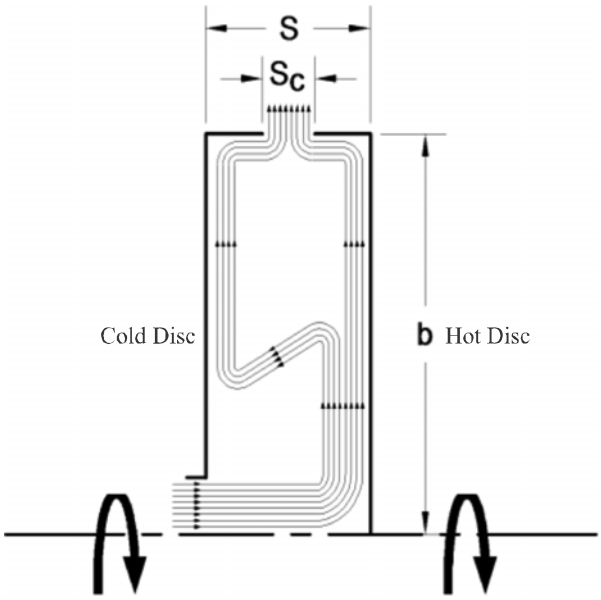

FIG. 1. SCHEMATIC DIAGRAMS FOR ROTATING CAVITY WITH RADIAL OUTFLOW

100°C near the outer edge of the disc, whereas temperature of the cold disc is similar to inlet air temperature of 20°C. Non-uniform and coarser meshing 75x92 in axial and radial direction respectively has been implemented for the simulations. For fine distributions of the grid nodes near the wall region, a distance of $y^+<0.5$ has been used, as shown in Fig. 2.

The HYBRID and HOUS (High Order Upwind Scheme), discretisation schemes have been adopted in combined form for the evaluation of the mean and fluctuating components at the control volume faces. To couple the pressure and velocity flow field and to satisfy the mass continuity within the system, a SIMPLEC (Semi-implicit Method for Pressure-Linked Equation of Consistency) algorithm of Van Doormal and Raithby [11] has been implemented.

3. TURBULENCE MODELS

Two turbulence models, the low Reynolds number k-ε model and the low Reynolds number second moment closure along with the energy equation have been employed. These models are built-in by default in the ANSYS Fluent CFD commercial code. Both the turbulence models are categorised according to the modelling of the Reynolds stress components, which are appeared in the time-averaging process of a Navier Stokes equations. The details of governing equations are given as:

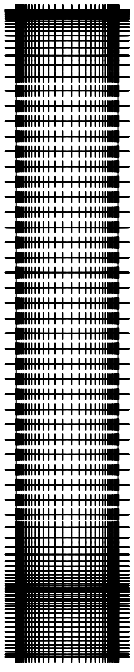

FIG. 2. NON-UNIFORM GRID

3.1 Low Reynolds Number k-ε Model

A well known low Reynolds number k-ε model which is based on the suggestions of Morse [12] has been used for the predictions. This model solves the turbulence quantities through the gradient transport hypothesis procedure, which is based on the transport equation for the kinetic energy (k) and its dissipation rate (ε):

$$\rho\overline{u_i u_j} = 2/3\delta_{ij}\,\rho k - \mu_T\left(\frac{\partial U_i}{\partial x_j}+\frac{\partial U_j}{\partial x_i}-2/3\,\delta_{ij}\nabla.\underline{V}\right) \tag{1}$$

where $\nabla.\underline{V}$ is the divergence of the velocity vector:

$$\nabla.\underline{V} = \frac{\delta U}{\delta z}+\frac{\delta V}{\delta r}+\frac{V}{r} \tag{2}$$

$2/3\delta_{ij}$ Normal stresses (i.e. i=j only)

3.2 Low Reynolds Number Second Moment Closure

The low Reynolds number second moment closure, which is based on the suggestions of Lai and So [13] has been adopted for the predictions. In this modelling procedure, an isotropic eddy viscosity approach is not invoked and the transport equations are resolved for each Reynolds stress component so-called Reynolds stress closure. The exact governing equation for the Reynolds stress components are expressed in Cartesian tensor as under:

$$\frac{\delta}{\delta X_k}\left(\rho U_k\overline{u_i u_j}\right)=\frac{\delta}{\delta X_k}\left(\overline{\frac{\delta u_i u_j}{\delta X_k}}\right)+\frac{\delta}{\delta X_k}\left(-\overline{\rho u_i u_j u_k}\right)$$
$$-\rho\left(\overline{u_i u_k}\frac{\delta U_i}{\delta X_k}+\overline{u_i u_k}\frac{\delta U_j}{\delta X_k}\right)-\overline{\left(u_i\frac{\delta p}{\delta X_j}+u_u\frac{\delta p}{\delta X_i}\right)}-2\mu\overline{\frac{\delta u_i}{\delta X_k}\frac{\delta u_j}{\delta X_k}} \tag{3}$$

or symbolically as:

$$C_{ij} = D^{v}_{ij} + D^{T}_{ij} + P_{ij} + \Pi_{ij} - \varepsilon_{ij} \quad (4)$$

where from left to the right can be read as convection, viscous diffusion, turbulent diffusion, production by mean strain, redistribution and diffusion due to the pressure interactions, and viscous dissipation of the Reynolds stresses respectively.

Modelling of the turbulent diffusion, pressure-strain interactions and viscous dissipation terms individually formed the exact equation for the low Reynolds number second moment closure, which represents the all the correlations in detail given as under:

$$C_{ij} \frac{\delta}{\delta X_k}\left[\mu \frac{\delta \overline{u_i u_j}}{\delta X_k}\right] + \frac{\delta}{\delta X_k}\left[\rho c_s \frac{k}{\varepsilon} \overline{u_k u_1} \frac{\delta \overline{u_i u_j}}{\delta X_k}\right] - \rho\left[\overline{u_j u_k} \frac{\delta U_i}{\delta X_k} + \overline{u_i u_k} \frac{\delta U_i}{\delta X_k}\right]$$
$$- \rho c_1 \frac{\varepsilon}{k}\left[\overline{u_i u_j} - 2/3\delta_{ij} k\right] - c_2\left[P_{ij} - 2/3\delta_{ij} P_k\right]$$
$$+ f_w\left[\rho c_1 \frac{\varepsilon}{k}\left(\overline{u_i u_j} - 2/3\delta_{ij} k\right) + \alpha\left(P_{ij} - 2/3\delta_{ij} P_k\right) - \rho \frac{\varepsilon}{k}\left(\overline{u_i u_k n_k n_j} + \overline{u_j u_k n_k n_i}\right)\right]$$
$$- 2/3\delta_{ij}\rho\varepsilon\left(1 - f_w\right) - f_w \rho \frac{\varepsilon}{k} \frac{\left(\overline{u_k u_j} + \overline{u_i u_k} n_k n_j + \overline{u_j u_k} n_k n_i + n_i n_j \overline{u_k u_1} n_k n_1\right)}{1 + 3\overline{u_k u_1} n_k n_j / 2k} - \frac{\overline{u_k u_j}}{k} D_k$$

For full detail see references, Abbasi, et. al. [14], Memon [3,15] and Lai and So [13].

3.3 Energy Equation

The generalized form of Reynolds-averaged energy equation for steady turbulent flow can be written in Cartesian tensor notation as:

$$\frac{\delta}{\delta xj}\left(Uj\phi\right) = \frac{\delta}{\delta xj}\left[\frac{\mu}{\Pr}\frac{\delta\phi}{\delta xj} - \overline{uj\phi}\right] \quad (5)$$

The cylindrical polar-coordinate form of the governing equations presented for the general variable (ε):

$$\frac{\delta}{\delta x}\left(U\phi\right) + \frac{1}{r}\frac{\delta}{\delta r}\left(rV\phi\right) = \frac{\delta}{\delta x}\left(\frac{\mu}{\Pr}\frac{\delta\phi}{\delta x}\right) + \left(\frac{r\mu}{\Pr}\frac{\delta\phi}{\delta r}\right) + s_{\phi} \quad (6)$$

Where the turbulent heat flux tensor emerged in Equation (5) is represented by the source term (ε).

4. DISCUSSION OF NUMERICAL RESULTS

The simulated results are presented for a rotating disc flows system for different values of rotational Reynolds numbers $Re_\theta = 6.13x10^5 \leq Re_\theta \leq 4.4x10^6$ and mass flow rates, $C_w \leq 28000 \leq C_w \leq 30000$.

4.1 Computed Flow Structure

Fig. 3(a-d) shows the predicted stream lines for the range of rotational Reynolds number $Re_\theta = 6.13x10^5 \leq Re_\theta \leq 4.4x10^6$ and the mass flow rates, $C_w \leq 28000 \leq C_w \leq 30000$. For the $Re_\theta = 6.13x10^5$ and mass flow rate, $C_w = 28000$, the incoming air directly strikes on the hot disc and developed a wall-jet along the disc, finally formed the Ekman layer in the outer part of the disc space. Remaining part of the air recirculated in inward direction to the cold disc and formed the recirculating cell of the air, which occupied the entire cavity. A comparison of both models illustrated that the k-ε model predicted the extra recirculating cell of the air in outer edge of the cavity. While the Reynolds stress model predicted a large cell and shows more influence in the source region. At 66% higher Reynolds number, $Re_\theta = 1.81x10^6$ and the same mass flow rate, the computed stream lines do not show the major change in the flow behaviour apart from the source region, which is elongated to outer region of the cavity due to buoyancy-induced effects as shown in Fig. 3(b). For 86% higher rotational Reynolds number $Re_\theta = 4.40x10^6$, the buoyancy-induced effects are more prominent and extended the flow structure in out ward direction. The assessment of the stream lines show that the low Reynolds number second moment closure predicted the larger recirculating cell of fluid than that of the k-ε model, however, k-ε model predicted three recirculating cells of the fluid as shown in Fig. 3(c). For 7% higher mass flow rate, $C_w = 30000$ and $Re_\theta = 1.85x10^6$, both the models predicted the contracted recirculating core of the fluid, which signifies that the buoyancy-induced parameter is affected by the higher flow rate as shown in Fig. 3(d).

4.2 Computed Static Temperature Contours

Fig. 4(a-d) presents the simulated temperature contours of two turbulent models for the range of rotational Reynolds number and mass flow rate, Re_θ=6.13x10 ≤ Re_θ ≤ 4.4x10^6 and C_w =28000 ≤ C_w=30000. At rotational Reynolds number, Re_θ=6.13x10^5 and the mass flow rate, C_w=28000. The predicted static temperature contours illustrated that due to direct impingement of the cooling air on the hot disc (downstream) formed a strong wall jet, which moves rapidly along the same disc. Due to swift movement of the fluid heat is not transferred to air properly at initial stage of the cavity. However, at higher radial location the air is recirculated from the hot disc to cold disc therefore, more heat has been transferred from the hot disc to cold disc up to outer edge of the cavity. Consequently, the temperature of the cooling air increased to maximum level at the outer edge of the cavity, as shown in Fig 4(a). For a 66% higher rotational speed, Re_θ=1.81x10^6, the major variation in the temperature distribution can be seen from the temperature contours of the hot disc and cold disc. This change in temperature distribution attributes the effects of higher buoyancy induced parameter which is increased at higher speed rotational, as shown in Fig. 4(b). For a 86% rotational speed, the cell of recirculating air is distorted in the outer part of the cavity therefore, the temperature distribution in this region is enhanced as compare to previous case, as shown in Fig. 4(c).

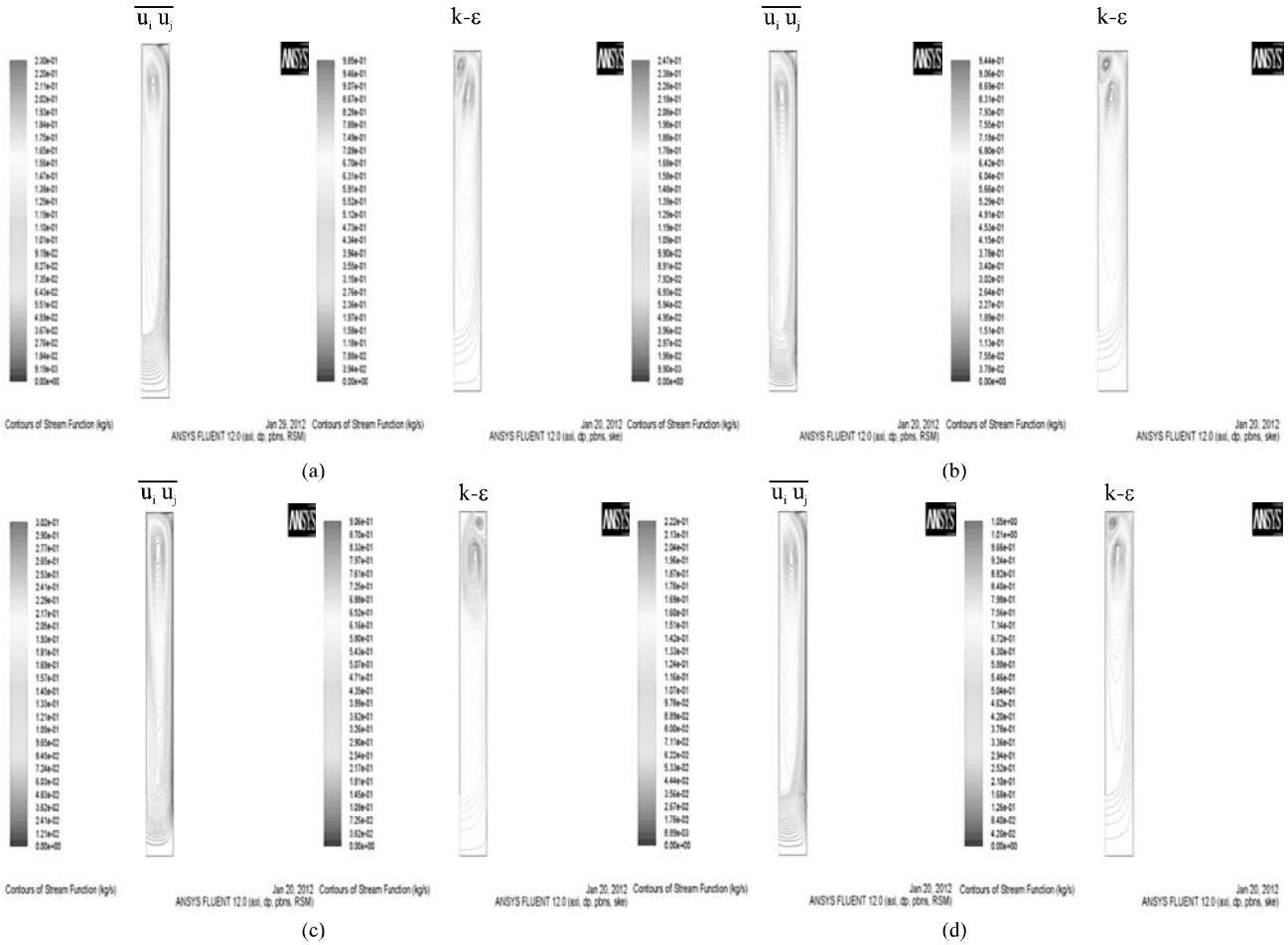

FIG. 3. COMPARISON OF COMPUTED FLOW STRUCTURES
(a) Re_θ=6.13x10^5 (b) Re_θ=1.81x10^6 (c) Re_θ=4.40x10^6 AND C_w=280000 (d) Re_θ=1.85x10^6 AND C_w=30000

For a 7% high mass flow rate, C_w=30000 at Re_θ=1.85x10^6, the buoyancy-induced parameter is less influential than the previous case. For this higher mass flow rate, a well developed strong wall jet has been formed along the hot disc. Therefore, recirculating cell of the fluid contracted in size and effect on the temperature distribution from the hot disc to cold disc, as shown in Fig 4(d). Overall comparison shows that for higher rotational speed the Reynolds stress model computed a stronger temperature distribution than the k-ε model (Fig 4(b)), which attributed that the former model is more capable than the later model to capture the higher operating conditions appropriately.

4.3 Computed Local Nusselt Number

Fig. 5(a-d) presents the comparison of computed local Nusselt numbers (Nu) for the hot and cold discs for a range of rotational Reynolds number 6.13x10^5≤ Re_θ ≤ 4.4x10^6 and the mass flow rates, 28000≤ C_w=30000 . The computed Nusselt numbers have been validated through the experimental measurements of the Mark-II rotating cavity rig at TFMRC (Memon [3]). The local Nusselt number can be expressed as:

$$Nu = \frac{rq_S}{k_I\left(T_S - T_I\right)} \tag{7}$$

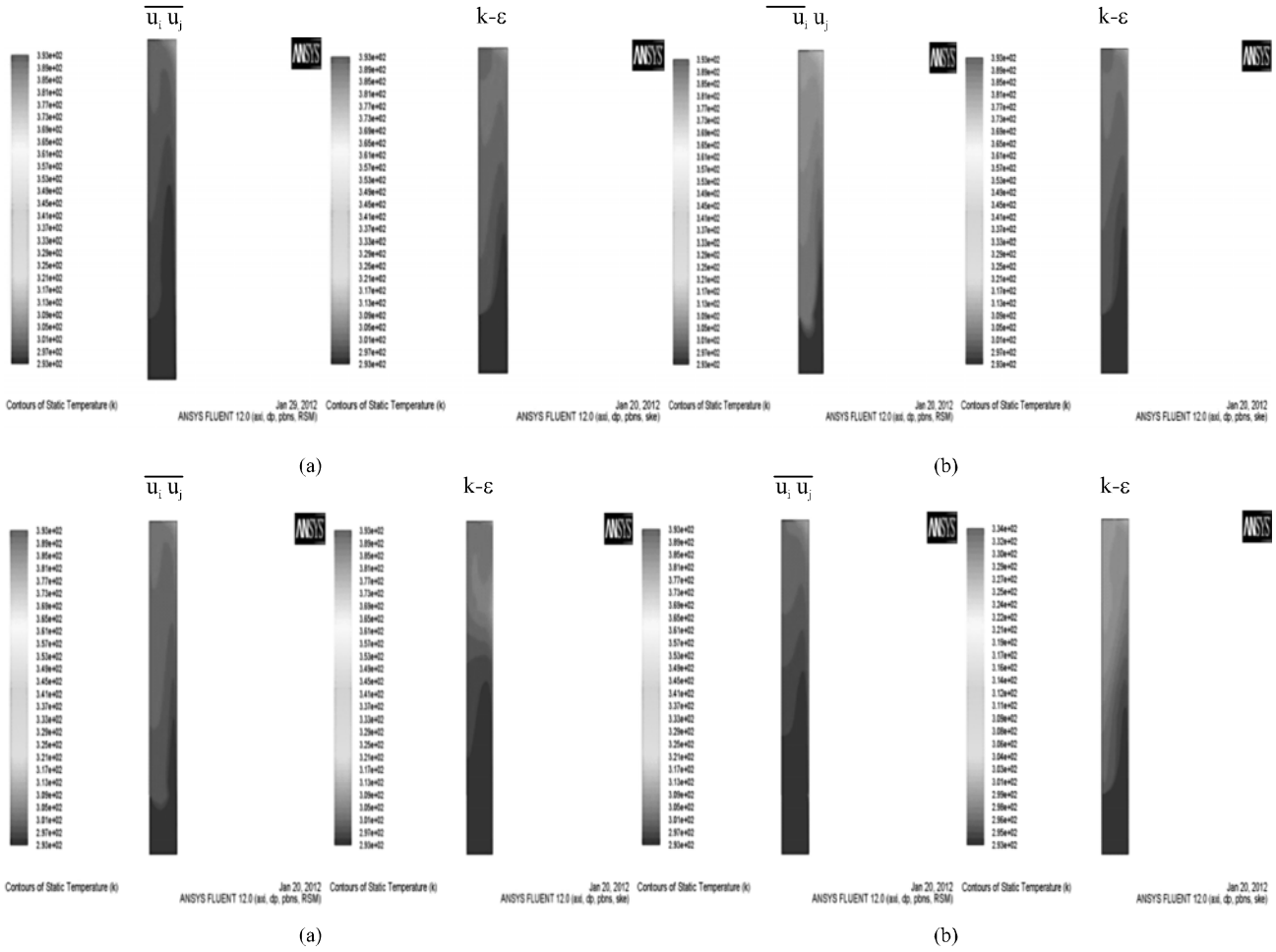

FIG. 4. COMPARISON OF COMPUTED STATIC TEMPERATURE
(a) Re_θ=6.13x10^5 (b) Re_θ=1.81x10^6 (c) Re_θ=4.40x10^6 AND C_w=280000 (d) Re_θ=1.85x10^6 AND C_w=30000

Where q_s and T_s are the heat fluxes and disc temperature at the disc surface respectively, and K_I and T_I and are the thermal conductivity and temperature of the inlet air.

The negative Nusselt numbers have been computed on the hot and cold disc at lower radial location for the rotational Reynolds number Re_θ=6.13x10^5 and mass flow rate, C_w=28000, as shown in Fig. 5(a). This trend reveals the lower temperature gradient between the incoming air and the first measurement position (r/b=0.323) on the upstream disc which varies from 296-302K. The temperature of the recirculating cooling air is higher than the cold disc; therefore, heat has been transferred from the recirculating air to the cold disc. Therefore, the negative Nusselt numbers have been computed at lower radial location of the cold disc. On other hand the predicted negative Nusselt numbers on the hot disc reveals that the incoming cooling air is not impinged on the downstream disc appropriately, while the temperature of the hot disc at lower radius is very low. For 66% higher rotational speed of Re_θ=1.81x10^6 at the same flow rate,

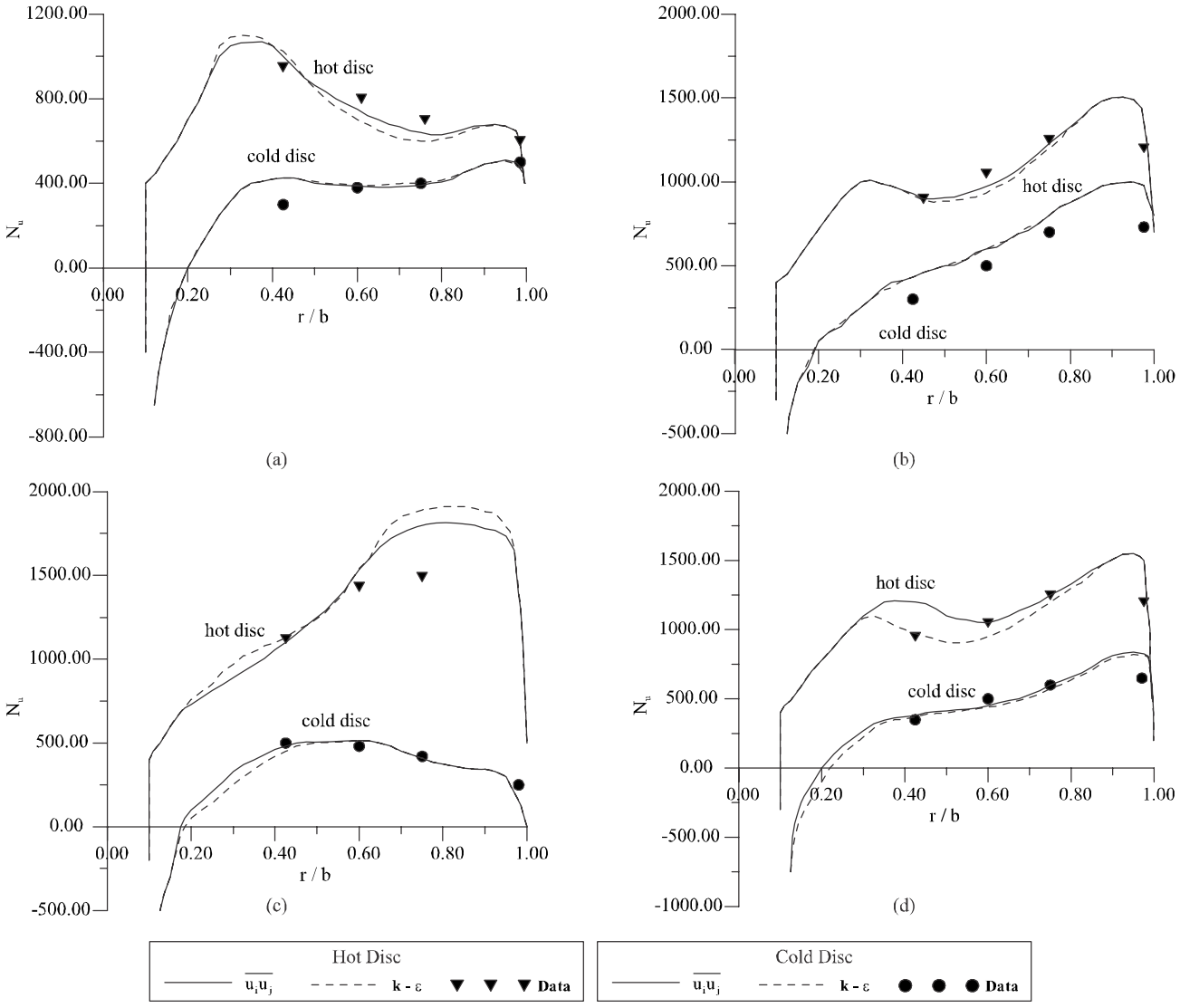

FIG. 5. COMPARISON OF LOCAL NUSSELT NUMBER FOR HOT AND COLD DISC
(a) Re_θ=6.13x10^5 (b) Re_θ=1.81x10^6 (c) Re_θ=4.40x10^6 AT C_w=280000 AND (d) Re_θ=1.85x10^6 AT C_w=30000

the incoming cooling air has been recirculated from the hot disc to cold disc and developed Ekman layers on the discs. The recirculation of the cooling air produced the weaker eddies in earlier stage of the source region and travelled from hot disc to cold one; consequently the heat has been transferred from hot to cold disc. Continuous enhancement in the Ekman layers increases the level local Nusselt numbers on both the discs, particularly on the hot disc. However, it is slightly decreased in the centre of the hot disc (downstream disc), as shown in Fig. 5(b).

The comparison shows the same variation in the local Nusselt numbers for both the discs. However, Reynolds stress model shows slightly better performance than the k-ε model in the centre of hot disc. For a 86% higher rotational speed, $Re_\theta=4.4x10^6$ a strong buoyancy effect has been observed which formed a large recirculation core of fluid and effected the entire flow structure and developed the non-entraining Ekman layers on both the discs. Therefore, the level of the local Nusselt numbers have been increased on both the discs, as shown in Fig. 5(c). This significant change in the local Nusselt numbers reveals the effects of buoyancy-induced parameter, which is increased on higher rotational speed and decreased on higher mass flow rate. Similar studies were made by Memon [3] and Owen, et. al. [8].

In contrast, for the highest flow rate, $C_w=30000$ the buoyancy-induced flow parameter is less influential than the lower mass flow rate ($C_w=28000$). Result of that the level of local Nusselt numbers have been decreased on the hot disc and increased on the cold disc in outer part of the cavity. This signifies that due to highest mass flow rate a strong wall-jet of air has developed along the hot disc which effects on the heat transfer from the hot disc to air. Overall assessment of computed results of both models demonstrates that the cold disc computations show a good agreement with measurements particularly for higher rotational speed and mass flow rate. However, both models underestimating at the centre of hot disc.

5. CONCLUSIONS

Numerical predictions have been carried out through the commercial CFD code ANSYS Fluent by invoking two low Reynolds number turbulence models for the range of rotational Reynolds numbers and mass flow rates. Predicted local Nusselt numbers of both discs show the negative values at initial stage and maximum at the outer part of the discs. Negative values of the local Nusselt numbers reveal the low temperature gradient between the incoming cooling air and the upstream disc and another possible reason is inappropriate impingement of the incoming air on the downstream disc. The significant effects of buoyancy-induced flow parameter have been observed on the computed flow structures, static temperature contours and Nusselt numbers. For the higher rotational Reynolds numbers the buoyancy-induced parameter is more influential than the lower one, which is characterised by an increase in the strength of the recirculating vortex. Consequently more heat was transferred from the hot disc to the cold disc. A comparison of the two models show that for higher rotational speed, the low Reynolds number second moment closure computed the buoyancy-induced effects more effectively than the k-ε model and showed a closer agreement with the experimental measurements. On the bases of discussion of result it is concluded that the low Reynolds second moment closure model can be used for the industry based complex geometries of higher operating conditions.

6. NOMENCLATURE

b	outer radius of cavity
$C_w = \dot{m} / \mu b$	non-dimensional mass flow rate
G = s/b	cavity gap ratio
k	turbulent kinetic energy
Nu	local Nusselt Number
p	static pressure
Pr	Prandtl number
q	heat flux
$Re_\theta = \Omega b^2/v$	rotational Reynolds number
r	radial coordinate
r/b	non-dimensional radial co-ordinate
r_i	inner disc radius
S	source term
s	axial gap between the discs
U,V,W	mean velocity components in z, r, θ
u,v,w	fluctuating velocity components in z, r, θ
$\overline{u_i u_j}$	Reynolds stress tensor
$y^+ = un_\tau/v$	wall-distance Reynolds number
z	axial coordinate
z/s	non-dimensional axial coordinate
ε	dissipation rate of turbulent kinetic energy
μ	dynamic viscosity
μ_T	turbulent viscosity
ϕ	generalised transport variable
Ω	rotational speed of the disc
ρ	density
δ_{ij}	Kronecker delta

ACKNOWLEDGEMENTS

The first author acknowledges Higher Education Commission, Ministry of Science & Technology, Government of Pakistan, for providing an opportunity and financial support to fulfil this work. Authors are also thankful to the Mehran University of Engineering & Technology, Jamshoro, Pakistan, for their encouragement and moral support.

REFERENCES

[1] Childs, P.R.N., Dullenkopf, K., and Bohn, D., "Internal Air Systems Experimental Rig Best Practice", ASME Paper GT2006-90215, 2006.

[2] Owen, J.M., and Onur, H.S., "Convective Heat Transfer in a Rotating Cylindrical Cavity", Journal of Engineering Power, Volume 105, pp. 265-276, 1983.

[3] Memon, M.D., "Numerical Modelling and Prediction of Fluid Flow and Heat Transfer in Rotating Disc Geometries", Ph.D. Thesis, University of Sussex, 1995.

[4] Mirzaee, I., Gan, X., Wilson, M., and Owen, J.M., "Heat Transfer in a Rotating Cavity With a Peripheral Inflow and Outflow of Cooling Air", Journal of Turbomachinery, Volume 120, pp. 818-823, 1998.

[5] Kilic, M., "Computation of Flow and Heat Transfer in a Rotating Cavities with a Peripheral Flow of Cooling Air", Annals of NY Academy of Science, Volume 934, pp. 513-520, 2001.

[6] Karabay, H., Wilson, M., and Owen, J.M., "Predictions of Effect of Swirl on Flow and Heat Transfer in a Rotating Cavity", International Journal of Heat and Fluid Flow Volume 22, pp. 143-155, 2001.

[7] Lock, G.D., Youyou, Y., Newton, P.J., Wilson, M., and Owen, J.M., "Heat Transfer Measurements Using Liquid Crystal in a Pre-Swirl Rotating-Disc System", Journal of Turbomachinery, Volume 127, pp. 375-381, 2005.

[8] Owen, J.M., and Powell, J., "Buoyancy-Induced Flow in a Heated Rotating Cavity", Journal of Turbomachinery, Volume 128, pp. 128-134, 2006.

[9] Owen, J.M., "Thermodynamic Analysis of Buoyancy-Induced Flow in Rotating Cavities", Journal of Turbomachinery, Volume 132, pp. 31001-31007, 2010.

[10] Vinod, K.B.G., Chew, J.W., and Hills, N.J., "Rotating Flow and Heat Transfer in Cylindrical Cavities With Radial Inflow", Journal of Engineering Gas Turbine Power, Volume 135, No. 3, pp. 32502-32514, 2013.

[11] Van, D.J.P., and Raithby, G.D., "Enhancement of the SIMPLE Method for Predicting Incompressible Fluid Flow", Numerical Heat Transfer, Volume 7, pp. 147-163, 1984.

[12] Morse, A.P., "Application of a Low Reynolds Number k-ε Turbulence Model to High-Speed Rotating Cavity Flows", Journal of Turbomachinery, Volume 113, pp. 98-105, 1991.

[13] Lai, Y.G., and So, R.M.C., "On Near-Wall Turbulent Flow Modelling", Journal of Fluid Mechanics, Volume 221, pp. 641-673, 1990.

[14] Abbasi, A.F., Memon, M.D., and Baloch, A., "Modelling and Predictions of Isothermal Flow Inside the ClosedRotor-Stator Flows", Mehran University Research Journal of Engineering & Technology, Volume 31, No.1, pp. 83-94, Jamshoro, Pakistan, January, 2012.

[15] Memon, M.D., Memon, A.A., and Jokhio, M.H., "Application of the Low Reynolds Number Second Moment Closure to the Closed Rotor-Stator Flows", Mehran University Research Journal of Engineering & Technology, Volume 18, No. 2, pp. 117-121, Jamshoro, Pakistan, April, 1999.